Unofficial supplement to Section 7.3 of Bacon et al. (2017): HST photometry of newly detected sources

Section authors: Mohammad Akhlaghi, Roland Bacon, Hanae Inami et al.

Reproduction pipeline v4-2-gf97e and Gnuastro 0.2.51-bc56-bugfix
on Tuesday 6th February, 2018, 23:10

1 Section 7.3 supplement

Accurate derivation of a target's spectrum, and emission line equivalent widths over the wide MUSE 3D cubes requires the target's spatial footprint (segmentation map) in broad-band images and also their broad-band magnitudes. The UVUDF survey (Rafelski et al. 2015, hereafter R15) catalog and segmentation map were the primary resource for this information. However, the wide field of MUSE offers the ability to detect targets based on spectral features for the first time. Therefore, in parallel to the R15 catalog, an independent 3D detection procedure was also applied directly to the MUSE datacube using the ORIGIN software.

[What was the total number of ORIGIN-only detections? In comparison with the 160 that were not in R15, this would be interesting completeness study and we might also check with NoiseChisel generated catalogs.]

The two independent catalogs were then matched [we need to add the search radius for the matching of ORIGIN results with R15 and possibly some other details, if it wasn't discussed in the section on ORIGIN.]. However, 160 of the ORIGIN detections did not corresponded to anything in the UVUDF catalog. Therefore, in Section 1.1 the list of objects is classified into various classes and in Section 1.2 the procedure to derive the segmentation maps and broad-band magnitudes for this list is discussed. All the results in this appendix are exactly reproducible and the reproduction pipeline is released with this paper[1].

1.1 Classification

An accurate analysis of the ORIGIN-only objects is necessary to confirm whether the absence of these objects in the R15 broad-band catalog is an artifact of the detection methods and configurations used, or it is indeed due to very weak (possibly non-existant) continuum emission. Given this independently derived list of objects (from the fundamentally different MUSE datacubes and different algorithm), this analysis can be very useful in analysing the causes of success or failure of the detection method used.

The objects can generally be classified into two classes: 1) Those with a footprint in the R15 segmentation map, but not in the catalog (Figure 1). 2) Those without a footprint in the R15 segmentation map (Figure 2). The R15 segmentation map and catalog was derived by applying SExtractor (Bertin and Arnouts 1996) to the average of all optical and near-infrared images and is a merger of several SExtractor runs with multiple detection and deblending paramters (see Table 2 or R15). Since these objects don't exist in the R15 catalog, a visual analysis was necessary, so 5″ cutouts were made (centered on the object) from the F775W image and the R15 segmentation map.

To understand the first class, it is important to recall that given the particular detection algorithm and input parameters used, non-zero pixels in a segmentation map correspond to the *detected* pixels. However, partial or full coverage (non-zero pixels) of the object's pixels in the segmentation map does not guarantee the object's existance in the catalog (as a unique object/row).

Figure 1 shows three categories of the first class of objects: 1.1) Those due to problems in deblending at a distance (first row). 1.2) Those due deblending problems of nearby objects (second row). 1.3) Those that were removed manually based on S/N and number of detections for high purity (third row). R15's primary reason for merging multiple SExtractor catalogs was to correct for the 1.2 category debleding problems (second row of Figure 1). However we see that 26.88% of the ORIGIN-only detections belong to this class. This failure is caused by a fundamental systematic bias in SExtractor's deblending methodology and has been thoroughly discussed in Appendix B.2 of Akhlaghi and Ichikawa (2015, hereafter AI15). The reasons for the first row of Figure 1 are also described there.

Figure 2 shows the second class of objects, the three categories for this class are: 2.1) Those that were detected by NoiseChisel in at least one of the filters (see Section 1.2). 2.2) Those where the diffuse flux was detected in the F775W filter, but no 'clump' could be specified for it. 2.3) Those that could not be detected by NoiseChisel. From Figures 1 and 2, it is clear that only 23.12% of the ORIGIN detected objects truely had very low continuum surface brightness to be detected as a separate (non-diffuse) entity. As reviewed above, this shows the methodological biases against reasonable completeness in R15's detection

[1] [Similar to Akhlaghi and Ichikawa (2015) where the reproduction pipeline is uploaded to arXiv along with the final paper's TEX sources. arXiv is the most reliable online place to store them with the paper (the whole pipeline is < 200kB). The pipeline can also be submitted to the journal.] The version controlled reproduction pipeline of this appendix is also available at https://gitlab.com/makhlaghi/muse-not-in-rafelski15.

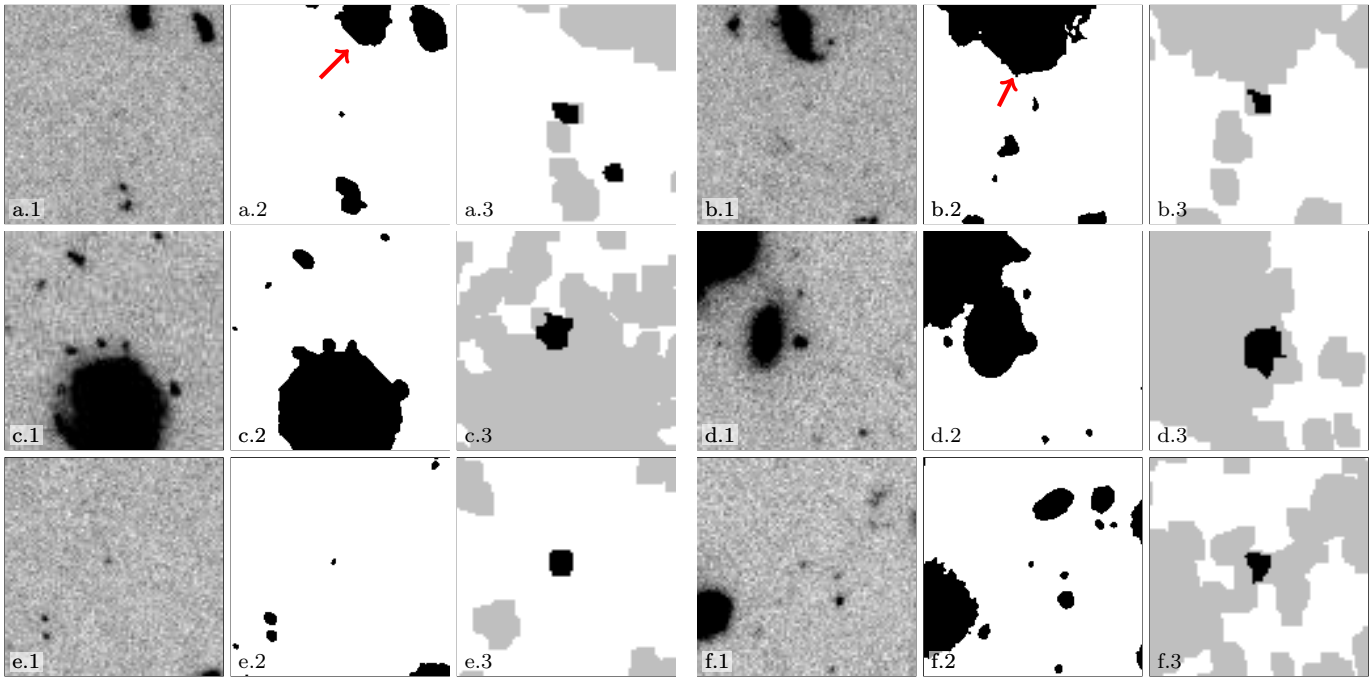

Figure 1: First class of ORIGIN detected objects that did not correspond to objects in the R15 catalog, but with footprints in the R15 segmentation map. The cutouts are 5″ wide and centered on the ORIGIN detections. The first column for each object (a.1, b.1, c.1, d.1, e.1 and f.1) are cutouts from the F775W image. The second column shows the non-zero (corresponding to an object) pixels in the R15 segmentation maps. The third column shows the NoiseChisel detections in the F775W image in gray and the black pixels show the final pixels used for this object (see Section 1.2). The first row (a and b) are spatially separated from other objects, nevertheless they have the same label as the object shown by the red arrow (also see Figure 17 of AI15). The second row (c and d) were too close to a much brighter object and thus not labeled differently. The third row (e and f) are objects with a unique label, but trimmed from from the R15 catalog for high purity (Section 5 in R15). These three classes constitute approximately 3.12%, 26.88%, and 5.62% of the ORIGIN-only detections respectively.

tools/parameters.

Note that 1 object (MUSE ID 6449) was outside of the field in the F775W images we were inspecting here for the classification, so it is not included in any of the percentiles mentioned above.

1.1.1 Corrections after publication

After the publication of (Bacon et al. 2017) and when preparing this pipeline for publishing, some very minor differences were found between this output and what was finally finished in the paper. As shown below, these differences are very minor and have no effect on our final result, but since the aim of this pipeline is *exact* reproduction, the differences must be described.

In the published results, the classification for object 6477 (MUSE ID) was not typed correctly and thus it was not included in the percentiles. This typo is now corrected. Finally, the percentiles in the published version were based on an input list of 173 objects. But that list was later (after giving the final results of this pipeline, and prior to publication) corrected to 160. It was my (MA) responsability to notice the change in the paper, but since it was a small change in the whole paper, I missed it and thus didn't update the pipeline's input or report a change in the output. Fortunately it only has a small effect on the percentiles. Therefore, it has no effect on the conclusions drawn from the percentiles. The input list in the pipeline now is the final list of 160 objects.

Another minor mistake found in the published paper is in the third paragraph of Section 7.3, we mentioned that "We inspect the 88 HST-detected objects discussed above ...". However, the number 88 (160 subtracted by the 72 aperture-based detection criteria) was a mistake. The processing that resulted in 72 objects was done with fixed apertures for all the objects and it was independent of this classification. Not noticing the new number 88 in this paragraph was my (MA) failure. This paragraph in the paper is about objects that were covered by a SExtractor segmentation map (the first class discussed in Section 1.1 above, Figure 1). From the percentiles of Figure 1, we see that this constitues 57 objects. So the first line of this paragraph must have been "We inspect the 57 ORIGIN-only objects that were covered by a detection in the Rafelski et al. (2015) segmentation map ...". Thefore, the three classes of Figure 1 constitute 8.77%, 75.44% and 15.79% of the 57% and these numbers are very close to those mentioned in the paper (namely 8%, 73% and 15%).

Finally, as noted in Figure 2, following all the corrections above, the value 39% that is discussed in the last paragraph of this section in the published paper should have been 40.62%. In the period after reporting these re-

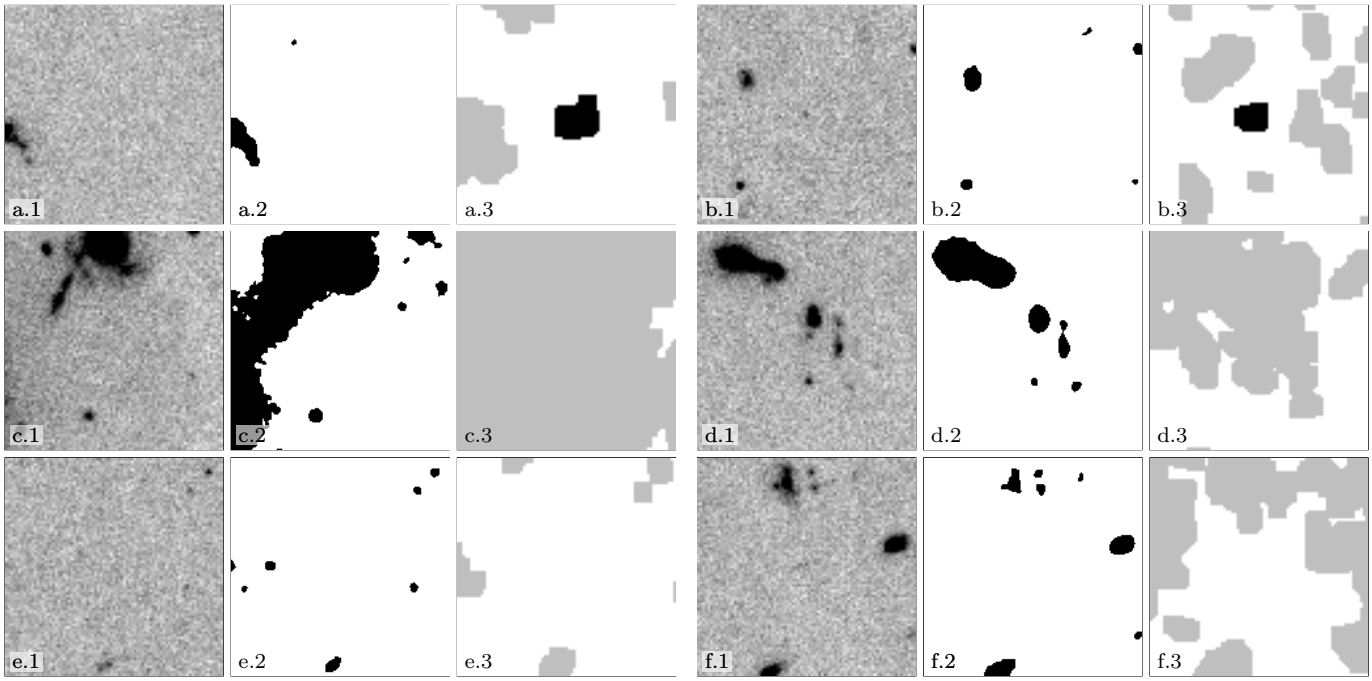

Figure 2: Similar to Figure 1, but for objects that were not covered by the R15 segmentation map. The first row (a and b) are objects that had a NoiseChisel detection. The second row are objects that were within NoiseChisel's detected regions, but could not be identified as a clump (their flux is blended too strongly with neighboring objects). The third row are example objects that could also not be detected by NoiseChisel. These three categories constitute approximately 40.62%, 15.00% and 8.12% of the ORIGIN-only detections respectively.

sults, I (MA) was heavily involved in the development of Gnuastro for our next projects with MUSE. Also, the concept behind this reproduction pipeline is also evolving very rapidly. These might have been partly the cause for these very minor mis-matches between this pipeline's results and those of the paper. In short these were human error and the future pipelines will be designed to mitigate the sources of this as much as possible.

1.2 Derivation of segmentation maps and broad-band magnitudes

The input 0.06″/pixel broad-band images were taken from the publicly available XDF[2] (Illingworth et al. 2013, for the optical and near infra-red images) and UVUDF[3] (R15, for the near UV images) surveys. In the IR images, the public XDF release is a multi-depth image containing the very deep single WFC3-IR field of view with the rest of the UDF area covered by shallower images. See Figures 3 and 4 in Illingworth et al. (2013) for the optical and IR exposure maps over the UDF.

Accurate detection and photometry require an approximately flat depth/exposure (or noise). Therefore, in the infrared, the deep and shallow regions were cutout and the full procedure below was done independently on each region[4]. Unfortunately the XDF survey has merged the shallow and deep regions into one image, therefore roughly 1/10th of the UDF area is covered by a very strong exposure/noise gradient. 13.8% of the ORIGIN-only objects lie on this gradient region. They have been flagged to note that their infrared magnitude error measurements are unreliable. [Discuss how R15 deals with this multi-depth region.] [Currently the images are not PSF-matched.]

As discussed above, approximately $\sim 26.88\%$ of the objects lie very close to a nearby neighbor along the line of sight in the R15 segmentation map (second row in Figure 1). With the much lower (sub-Sky) thresholds of NoiseChisel, this number greatly increases. For example compare the gray regions of third column in Figures 1 and 2 with the black regions of the second columns. Most commonly these much larger and brighter neighbors are lower redshift galaxies, with no physical proximity to our desired target. To avoid the effect of the neighbor's diffuse and large wings on the shape and thus measured photometry of these objects we use NoiseChisel's "clumps" to identify their pixels (see Section 3.2.1 of AI15). The boundaries of clumps in NoiseChisel are defined by the 2D noise fluctuations and

[2] https://archive.stsci.edu/pub/hlsp/xdf
[3] https://archive.stsci.edu/pub/hlsp/uvudf/v2.0
[4] The south, east, north and west vertices of the UDF field are respectively chosen to be at (53.164378, −27.835015), (53.113940, −27.792366), (53.161102, −27.748101), and (53.211670, −27.789811). This area covers the full R15 segmentation map. The vertices of the deep infrared XDF region are defined in https://archive.stsci.edu/prepds/xdf and located at (53.187414, −27.779152), (53.159507, −27.759633), (53.134517, −27.787144), and (53.190904, −27.778703). The deep/shallow boundary region with strong gradients is outside the deep infrared XDF region but inner to these vertices: (53.162129, −27.810275), (53.130682, −27.787376), (53.158913, −27.756522), and (53.190904, −27.778703).

therefore locate the region were the diffuse neighbor's wings start significantly influencing the total pixel flux.

When there is no nearby neighbor, the diffuse flux (that has been detected) can unambiguously[5] be used in the object's photometry. To implement this, the following strategy is adopted: when a detection is covered by more than one clump, the clump's segmentation map is used. However, when the detection has only one clump or no clumps at all (a very diffuse object), we use the full detection's segmentation map for that object[6]. For more on the distinction between detections and clumps, please see Sections 3.1 and 3.2 of AI15[7]. Finally, since the existance of these objects is known a-priori (independent of these broad-band images, in other words, there is no purity problem) we have set `--detquant=0.90`, and `--segquant=0.90` to increase completeness. [Add the NoiseChisel configuration file.]

Figure 3 shows the magnitude difference between R15 and our run of NoiseChisel (with the configuration discussed above) on the F775W image. In the case of brighter objects, R15 has measured a brighter magnitude (bottom half mostly filled) for some objects compared to NoiseChisel. This confirms the success of the configuration discussed above: diffuse flux is more common around large/brighter objects. By ignoring the diffuse flux when there is more than one clump (to detect and measure the magnitudes of the first row in Figure 1), we measure a fainter magnitude. The deblending problems of SExtractor near bright objects also contributes to this brighter magnitude. For the fainter objects, it is clear how at fainter limits, we have detected a brighter magnitude compared to R15. This is due to NoiseChisel's exceptional ability to dig deeply into the noise and detect the fainter flux. Compare the sizes of the regions between the second and third columns of Figures 1 and 2. [Currently the labeled segments in the final segmentation map are treated as objects (even if they were clumps originally) so the flux of the river pixels around the clumps is not subtracted. To be very precise we have to subtract the river pixel's flux from the clumps.]

To obtain the magnitudes of the ORIGIN-only (input) detected objects, NoiseChisel is run with this configuration on all the filters individually. The resulting catalog is then matched with the input catalog. Matching is defined as the nearest object within 0.30″ of the input catalog. The largest segmentation map (from all the filters that have a match) is used to represent the spatial footprint of each

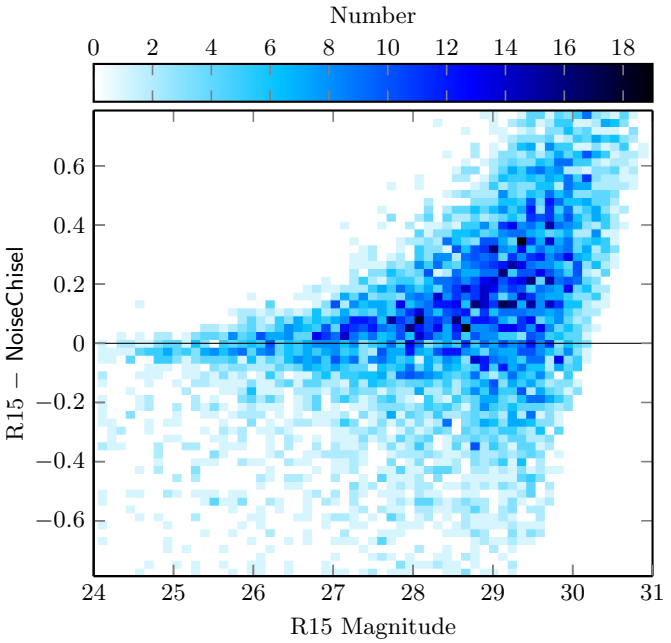

Figure 3: Magnitude difference as a function of magnitude, for 7583 objects in Rafelski et al. (2015) that are within 0.18″ of our NoiseChisel run's detections.

input object. If an object could not be matched with a detection on any of the filters, an aperture with a diameter of 0.50″ is positioned on the given coordinate. This gives a uniquely labeled region for each ORIGIN-only detected object which are then merged into one segmentation map. [Due to the narrower PSF of the ACS filters, ideally the segmentation map of ACS filters needs to be convolved with a matching kernel to be used on WFC3 filters.]

The segmentation map is fed into MakeCatalog along with the input, Sky, and σ_{Sky} of each filter to generate the final catalog. [Currently the Sky and σ_{Sky} images are taken from the first run of NoiseChisel on each image. We need to add an extra run tailored for an accurate Sky and σ_{Sky} measurements.] [Also, the images are not currently PSF-matched, so the unified segmentation map is not measuring exactly the same area of the sky. Ideally, we should use one segmentation map from ACS and WFC3/UV images and one for WFC3/IR images.]

As lower magnitudes are measured, the observational scatter caused by the noise can greatly harm the robustness of the result. Therefore when an object's magnitude is below a certain limit, the magnitude is replaced with an upper limit magnitude. Given the different (correlated) noise properties of each image and very large range of sizes and shapes that are found or set for the objects, a fixed value cannot be used as an upper limit magnitude for all the objects. Therefore we also call MakeCatalog's `--upperlimitmag` column in this run. When asked for this column, MakeCatalog will take the object's segmentation map and shift it to various random positions over the undetected areas of the image and will measure the magnitude until 200 magnitudes are measured for that object over the blank ar-

[5] 'Unambiguous' is used in reference to the particular image's depth and resolution. Much deeper and higher resolution images (for example by JWST) might reveal substructure.

[6] The following NoiseChisel options were set to achieve this behavior: `--grownclumps`, `--gthresh=100000`, `--objbordersn=1000`.

[7] As a review, in the signal-based paradigm (which was exclusively used in astronomy until now) peaks are first found and used to estimate/model the fainter parts that are buried in noise. So there is no distinction between (true) peaks and detections. However, in the noise-base paradim, a detected region is first found using a threshold that is far below the Sky value. The detected region is hence found independently of the brightness structure above the Sky value. Afterwards, true peaks ("clumps") are found over the detected region. Thus a detection region can have no peaks.

eas of the image. The upper limit magnitude for that object is then taken as a multiple (3 in this case) times the standard deviation of this distribution[8]. When the measured magnitude of the object is below this limit, this upper limit magnitude is used instead.

References

Akhlaghi, M. and T. Ichikawa (Sept. 2015). ApJS, 220, 1.
Bacon, R. et al. (Nov. 2017). A&A, 608, A1.
Bertin, E. and S. Arnouts (June 1996). A&AS, 117, 393.
Illingworth, G. D. et al. (Nov. 2013). ApJS, 209, 6.
Rafelski, M. et al. (July 2015). AJ, 150, 31.

[8] To decrease the effect of strong outliers, the upper limit is actually found after σ-clipping: all objects beyond 3σ are clipped until the relative change in σ is below 0.2. See Section A.3 in AI15.